journal

J. Am. Ceram. Soc., ■■ [■■] 1–7 (2011)
DOI: 10.1111/j.1551-2916.2011.04561.x

A Shape-Morphing Ceramic Composite for Variable Geometry Scramjet Inlets

Richard Miles,† Phillip Howard, Christopher Limbach, and Syed Zaidi

Department of Mechanical and Aerospace Engineering, Princeton University, Princeton, New Jersey 08544

Sergio Lucato, Brian Cox, and David Marshall

Teledyne Scientific Company, Thousand Oaks, California 91360

Angel M. Espinosa, and Dan Driemeyer

Boeing Phantom Works, Saint Louis, Missouri 63166

The development of ceramic composites with three-dimensional fiber reinforcement architectures formed by textile methods has led to the potential for active shape-morphing surfaces that can operate in high temperature and variable pressure environments. This technology is of particular interest for hypersonic applications, where SCRAM jet engines require variable inlet geometry to achieve efficient flight over realistic flight profiles and variable flight conditions. The experiments reported here show that significant shape morphing can be achieved and good control of the shape sustained even in the presence of large temperature and pressure gradients. Experiments were carried out using a subscale morphing hypersonic inlet with rectangular cross-section in a Mach 8 wind tunnel facility with a total temperature of 800 K. The upper surface of the inlet consisted of a C–SiC composite plate (0.7 mm thick, 37.5 cm long, and 11 cm wide) connected to five actuators through a triangular truss support structure. The lower surface was a flat plate instrumented with an array of pressure taps along the flow centerline. As the shape varied, the surface contour was reliably controlled for high efficiency, low loss compression. A factor of six inlet area ratio variation was achieved and good agreement with model predictions was observed.

I. Introduction

High-temperature shape-morphing structural materials could potentially revolutionize the design of air breathing hypersonic vehicles. The performance of the RAM/SCRAM engine is strongly affected by shapes and contours of the compression ramp and inner surfaces, including the inlet, the isolator, the combustor and the nozzle.[1,2] A contour that is designed for operation at one Mach number can be very inefficient at off-design Mach numbers. Even weak shock waves can substantially reduce engine performance, while instabilities in the flow can lead to upstream shock motion and engine unstart. High-temperature shape-morphing materials could (i) enable continuous variation of the inlet area ratio to accommodate changing Mach number and air density associated with climb and descent; (ii) improve engine and isolator performance by accommodating area and shape changes associated with engine mode transition from subsonic to supersonic combustion (RAM to SCRAM); (iii) optimize the compression ramp and inlet contour to minimize shock formation and reduce pressure losses; (iv) permit dynamic adaptation to compensate for flight maneuvers and correct for distortion due to thermal expansion, as well as suppress upstream shock motion to reduce the probability of engine unstart, and if unstart occurs, reduce the recovery time; and (v) improve nozzle performance by controlling the nozzle area ratio and contour for efficient thrust generation and minimum pressure loss. On both internal and external surfaces of the vehicle, high-temperature morphing materials could replace hinged control surfaces with smoothly varying surfaces, thereby eliminating flow disturbances associated with discontinuous changes in slope.[3]

High-temperature shape-morphing materials are also of interest for hypersonic and supersonic ground test facilities.[4] In this case, the shape-morphing capability would allow for dynamic optimization of the expansion contour of the facility, improving the flow quality, reducing shock and expansion waves and thus minimizing losses and improving performance. Shape morphing would also provide the opportunity for real time control of the facility Mach number by changing the expansion area ratio continuously. Low-temperature variable Mach capability has been previously demonstrated for a Mach 2.5–3.2 in-draft wind tunnel nozzle.[5] This leads to the possibility of simulating portions of the flight mission including climb and descent. Asymmetric shape morphing can be used to simulate asymmetric inlet flows for direct connect engine test applications.[6] Optimizing the performance of flow deflectors and other aero appliances and the diffuser is also important for ground test facilities because they affect the flow quality and the pressure recovery and thus the facility operating envelope and run time. High-temperature shape-morphing aero appliance surfaces and diffuser geometries could accommodate configuration variation of test articles and allow for dynamic changes to occur during the ground test, such as changes in angle of attack.

To operate in these applications, a high-temperature shape-morphing material must be both flexible and structurally stiff, with strength sufficient to withstand the stresses associated with high thermal gradients and pressure gradients. The material must be capable of withstanding temperatures in excess of 1500 K for even modest Mach numbers (Mach 8), resistant to oxidation, and resistant to thermomechanical fatigue. The purpose of this paper is to describe the design and fabrication of a shape-morphing ceramic composite (CMC) structure that satisfies these requirements and to present results of preliminary testing of its performance under hypersonic conditions, as the wall of a subscale inlet in a Mach 8 wind tunnel.

B. McMeeking—contributing editor

Manuscript No. 29043. Received December 13, 2010; approved March 9, 2011.

Funding at Princeton was provided by the Office of Naval Research Multi University Research Initiative through the University of California, Santa Barbara. Funding at TSC was provided by Boeing Phantom Works for development of the morphing CMC structures and by the Air Force Office of Scientific Research and NASA through the National Hypersonic Science Center for Materials and Structures for collaboration during testing at Princeton.

†Author to whom correspondence should be addressed. e-mail: miles@princeton.edu

II. CMC Structure

(1) General Design Considerations for Morphing Ceramic Composite

The challenge of designing morphing surfaces that are sufficiently flexible to change shape by bending or twisting yet capable of supporting large pressure loads has been addressed by combining thin face sheets with stiff, statically determinate truss structures.[7–10] A class of those high authority shape-morphing structures has been initially described by Lu *et al.*[11] and further generalized by Hutchinson *et al.*[10] Previous studies have also suggested that these face sheet truss structures are a lighter-weight alternative to metallic foam core structures.[12] A simple example building on Lu's work is shown in Fig. 1, where a thin face sheet attached to a triangular truss structure is actuated by heating selected truss elements with an electric current. The active elements consist of a shape memory alloy, which undergoes a reversible strain on heating and cooling. This class of morphing structures can be actuated by internal active elements, as in Fig. 1, or by forces applied externally. Previous studies have been directed at optimizing morphing structures with other truss structures capable of more intricate shape changes with metallic or polymer face sheets.[7–10]

With recent advances in forming textile-based CMCs,[10] hybrid systems consisting of a CMC face sheet attached to metallic truss structure are also feasible. In this case, with the high-temperature CMC face sheet facing the hot gas flow, the temperature of the metallic truss structure may be controlled if necessary by active or passive cooling to maintain sufficient temperature gradient across the hot face sheet. Structures of this type are enabled by several characteristics of textile-based composites. One is the ability to form mechanically robust thin skins with through-thickness fiber reinforcements that eliminate delamination as a failure mode. Thin C–SiC and SiC–SiC composite skins (thickness <1 mm) with woven reinforcement architectures have been fabricated and shown to survive combustion environments with surface temperatures of 1800 K and temperature gradients >1000 K/mm across the hot skin.[13] The face sheet of the structure in Fig. 1 consists of such a composite (SiC–SiC), with two-layer, angle-interlock reinforcement architecture.[14]

The other enabling characteristic is the ability to form arrays of connections between the backside of the hot skin and the truss structure capable of transmitting both tensile and compressive loads. A simple example of a smoothly pinned joint, from the structure in Fig. 1, is shown in Figs. 2(a) and (b). The connectors consist of fiber tows drawn out from the weave structure of the composite skin to form loops held in shape by carbon rods during weaving of the fiber preform. After using chemical vapor infiltration (CVI) to deposit a thin coating of BN on all the fibers (which serves as a debond layer to enable toughening), the preform was rigid and the carbon rods were removed. The SiC matrix was then infiltrated into the preform, a superalloy wire was inserted into the loops, and the truss elements were attached to the wire by laser welding.

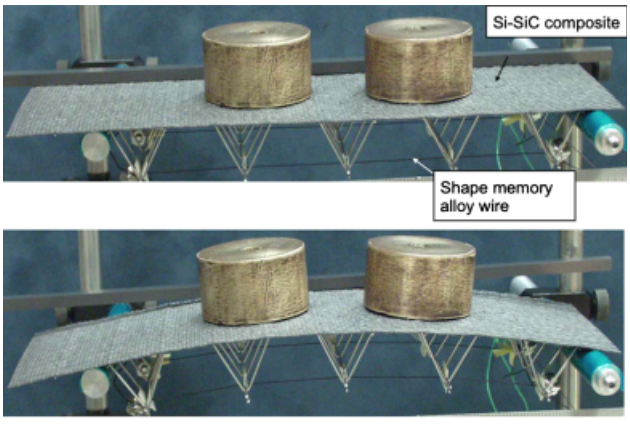

Fig. 1. Shape-morphing structure with SiC–SiC face sheet, superalloy support structure, and shape memory actuating struts.

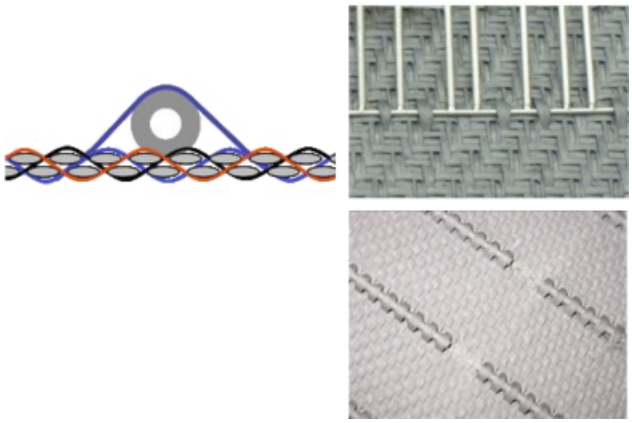

Fig. 2. Smoothly pinned joints connecting CMC skin and truss structure: (a) schematic of weave structure; (b) configuration used in the morphing structure in Fig. 1 with superalloy struts attached; (c) configuration used in the morphing structure in Fig. 3.

The maximum load capability (or lifetime in oxidizing environments) of the attachment feature shown in Fig. 2(b) is limited by damage generated by local stress concentrations at the contact between the superalloy wire and the inside of the CMC loops. A more robust design is shown in Fig. 2(c). In this case, the fiber tows forming the connectors were drawn over molybdenum tubes (outer diameter 2 mm, inner diameter 1 mm) during weaving. The tubes remained in place during subsequent processing of the composite, whereupon selected sections of the tubes between the loops were cut and removed, leaving the sections of the tubes beneath the loops as an integral part of the attachment structure. The insides of these tube sections provide a smoother, better aligned, and more damage resistant bearing surface for the superalloy rods.

The achievable deflections of a structure such as Fig. 1 are dictated by the face sheet thickness and strain limit. The critical radius of curvature ρ_c for bending of an initially flat face sheet is given by

$$\rho_c = \frac{t}{2\varepsilon_c} \tag{1}$$

where t is the face sheet thickness and ε_c the critical strain. CMCs generally show relatively high fatigue limits in cyclic loading.[15,16] If we take a conservative limit $\varepsilon_c \sim 0.25\%$, less than half of the typical failure strain for SiC–SiC and C–SiC composites, the minimum radius of curvature for a face sheet of thickness of 1 mm is ~ 200 mm. The radius of curvature in Fig. 1(b), with center deflection of 19 mm, is ~ 600 mm.

(2) Fabrication of morphing duct

A morphing CMC structure that would serve as the top wall of a model inlet duct of length 37.5 cm and width 11 cm was constructed as shown in Fig. 3. The CMC skin was fabricated using a woven preform of carbon fibers (T300-3K) with a two-layer angle-interlock structure and attachment sites formed with the method shown in Fig. 2(c). The composite was processed by CVI in two steps, the first to deposit a coating of pyrolytic carbon (~ 0.5 μm thickness) on individual fibers, and the second to form a matrix of SiC.

The supporting metal truss structure, consisting of a triangular array of solid superalloy plates, was connected to the CMC skin with superalloy rods passing through the molybdenum tubes of the attachment sites and matching holes in lugs that had been cut at the edges of the plates in a hinge-like configuration. This structure is easily flexed in the longitudinal direction but has high stiffness in the lateral direction.

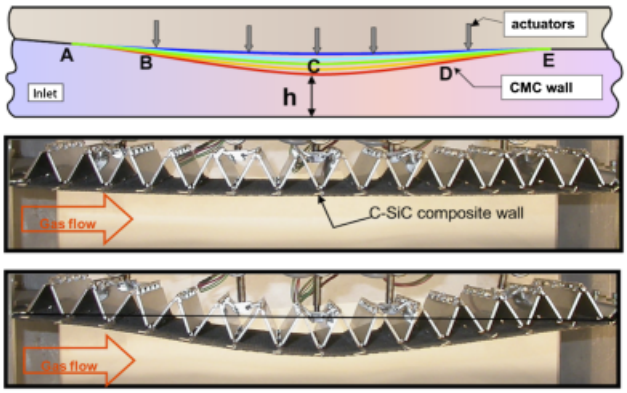

Fig. 3. Subscale morphing inlet. (a) Schematic showing sequential target shapes of top CMC wall during morphing; (b) and (c) side view of inlet showing CMC wall in positions for maximum and minimum inlet area ratio.

The target family of deflected shapes for the wall, illustrated in Fig. 3(a), was achieved using five actuators connected to the support structure through pivot plates visible in Fig. 3. The actuator rods were driven by stepper motors controlled through a Labview program, so that all actuators moved in synchronization and the shape transitioned smoothly between successive contours. The position control relied on simple counting of steps in 3.05 μm/step increments starting from an initial calibrated reference state. The family of shape contours satisfied the constraints that the morphing CMC section of the duct must transition smoothly at the ends to a mating fixed metallic structure (i.e., the slope at positions A and E remained fixed during all actuation movements) and that the deflections in the central throat region (C) extend over a range of 25 mm. At the extreme position Fig. 3(c), the radius of curvature of the CMC wall is approximately 250 mm in the throat region (C) and approximately 500 mm at positions B and C. Note that while the actuator displacements are in the same direction at positions B, C and D, the forces applied at the CMC skin are compressive at position C and tensile at positions B and D.

III. Wind Tunnel Testing

A Mach 8 wind tunnel at Princeton University was used to assess the potential of the composite structure in Fig. 3 for hypersonic morphing applications. Issues to be examined include the performance of the material under thermal stress, the flow quality achievable, the performance of the actuators, the impact of pressure gradients on the material, including start up and shut down transients, the stiffness and dynamic stability of the material in the presence of high frequency buffeting from a hypersonic flow, and the ability of the material to deflect sufficiently far and sustain a specified contour sufficiently well to control the flow without leakage or mechanical damage. The wind tunnel operates at a total temperature of 790 K and at a stagnation pressure of 1050 psi (7.24 MPa). The tunnel is operated with an air ejector system and can be run for several minutes at a time, limited by the capacity of the electrically driven storage heater. At Mach 8, the static temperature is $\sim$60 K and the static pressure is $\sim$5 Torr (0.28 kPa). The tunnel has a 9 in. (23 cm) diameter circular test section.

The morphing CMC skin of Fig. 3 was mounted in the fixture shown in the inset of Fig. 4, which formed a rectangular duct with fixed side walls and base plate beneath the morphing CMC top wall. The upstream end of the CMC skin was held in a fixed position against the mating inlet ramp on the tunnel wall, while at the downstream edge sliding occurred between the CMC face sheet and the mating metal duct surface during actuation. The side walls were quartz to allow optical observations during testing. The fixture was placed at the top of the tunnel, with bypass air flowing below it to avoid choking of the tunnel itself. Figure 4 is a schematic of the wind tunnel showing the location of the test fixture.

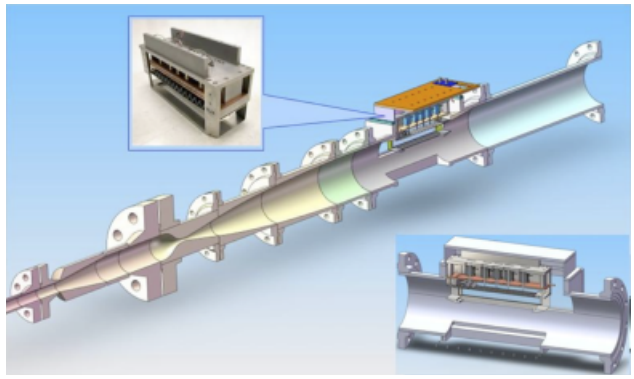

Fig. 4. Diagram of the Princeton Mach 8, 800 K, 1050 psi (7.24 MPa) facility showing details of the morphing inlet insertion and the morphing inlet geometry. A copper plate is placed between the surface and the five actuators to isolate them from the high temperature. Inset shows morphing inlet seen through the schlieren side windows.

As the flow is compressed in the morphing inlet, the pressure increases significantly above the free stream static pressure. The pressure at the back of the morphing surface is determined by the downstream static pressure, which remains well below the pressure of the air in the inlet duct, leading to an outward compressive force on the actuators. This force increases nonlinearly as the morphing surface approaches the opposite wall. The pressure in the duct ranged from about 0.5 psi to $\sim$14 psi (2.5–100 kPa). The edges of the morphing wall were not sealed against the side walls (the clearance was $<$0.5 mm), so some air leakage occurred from the duct to the backside cavity. However, the leak rate was sufficiently small that there was very little perturbation to the flow inside the duct.

Because the actuator driver rods could not be conveniently vacuum sealed from the morphing surface in this particular setup, the entire structure including the actuators and driving electronics was enclosed within the wind tunnel test chamber, as shown in the Fig. 5. A 7° inlet ramp was installed from the top of the curved tunnel wall to divert the flow into the morphing section. The leading edge of the morphing plate was mounted at a 5° angle to minimize discontinuity and shock formation at the joint with the inlet ramp. The rear of the morphing section was captured into a sliding retainer. The back end of the actuator section was left open to the tunnel diffuser so that large pressure gradients would not occur across the morphing panel during

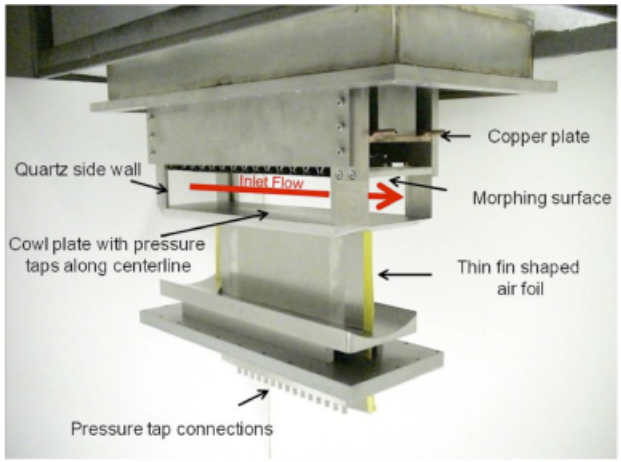

Fig. 5. Morphing inlet tunnel model including the 13 pressure taps that are routed to the bottom of the wind tunnel through a thin fin. The water-cooled copper plate can be seen near the top. The curved boundary beneath the air-foil mates flush with the wind tunnel's inner perimeter.

start up and shut down. Even though the static temperature of the air in the test section is low, the boundary layer and other stagnant air rises to a temperature close to the total temperature of the plenum (800 K). Because the stagnant hot air permeates the chamber behind the morphing panel, a water-cooled copper thermal insulation plate was installed between the CMC wall and the actuators to protect the actuators from the high temperatures.

In order to quantify the static pressure profile, a series of 13 pressure tap holes were drilled along the centerline of the flat bottom plate at 16 mm intervals. The pressure tap tubes were routed across the hypersonic flow below the flat plate to the bottom of the wind tunnel through a thin fin-shaped air-foil to minimize disturbance of the wind tunnel below the inlet flow. The fin structure, with a bottom curved plate that fits the contour of the lower section of the wind tunnel, is shown in Fig. 5. The diagnostics included the static pressure profile from the 13 pressure taps as well as schlieren images of the shock structure taken through the side windows and an overall video of the motion of the surface.

IV. Flow Modeling

Initial modeling of the inlet was undertaken using the proprietary Boeing 3D BCFD flow solver, assuming laminar adiabatic flow. This modeling was undertaken to assure that the insertion of the morphing inlet did not choke the wind tunnel and to determine the impact of the tunnel boundary layer on the inlet flow field. The flow solver computed the flow along the entire wind tunnel, following the expansion contour from the throat of the tunnel through the test region. The flow was solved for half of the tunnel using 6.3 million cells assuming a symmetry plane. The computation was performed for the flow from the nozzle throat through and below the morphing inlet and it included the boundary layer evolution. Because of the conservation of enthalpy and entropy in an ideal expansion, the plenum has to be operated at high temperature and pressure to provide the kinetic energy and dynamic pressure required for testing. For the tests conducted here, the objective was to create a Mach 8 simulation so that aerodynamic properties of the flow including shock and expansion wave structure could be determined. Even though the proper Mach number is reached, the facility is not capable of producing the true flight air speed and static temperature because that requires plenum temperatures on the order of 2500 K. For Mach number duplication what is necessary is to have high enough plenum temperature to avoid condensation of the air as it cools by a factor of almost 14 in the expansion. The pressure drops by a factor of $\sim$10 000 (assuming ideal gas with a ratio of heat capacities of 1.4). Modeled conditions at

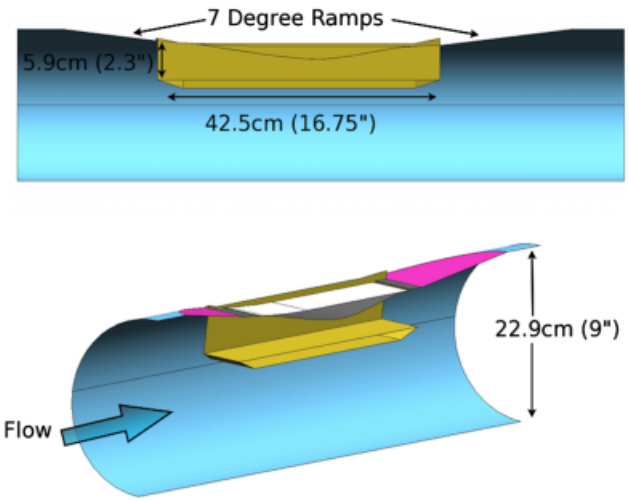

Fig. 6. Wind tunnel geometry used for the Boeing 3D BCFD code computation.

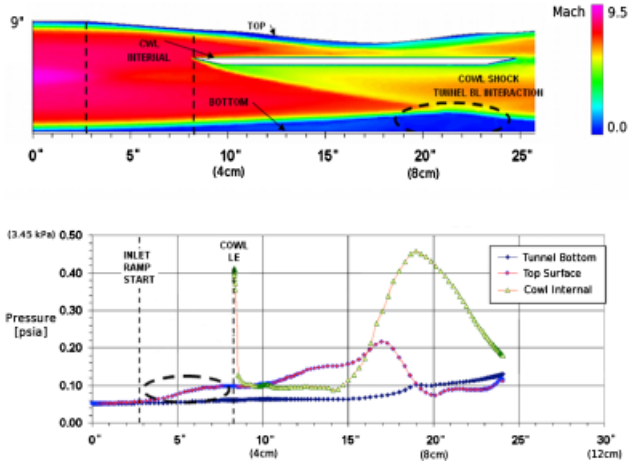

Fig. 7. (a) Mach number field around the test section. (b) Surface pressures computed for Mach 8 flow. All simulations were done using the Boeing 3D BCFD code with laminar flow.

the throat of the tunnel were 800 K (1440 R) and 450 psia (3.1 MPa), corresponding to plenum conditions of 960 K (somewhat higher than actual operating conditions of the facility) and 860 psi (5.9 MPa) (somewhat lower than the actual operating conditions of the facility). The geometry used for the modeling is shown in Fig. 6. This inlet geometry was an earlier configuration with the cowl plate located 2.31 s (59 mm) from the flat morphing surface. For the run reported here, the location of the cowl plate was 1.2 s (30 mm) below the flat morphing surface, significantly closer to that surface so a more substantial compression ratio could be achieved.

Figure 7 shows the predicted centerline Mach numbers (7a) and the wall pressure profiles (7b) of the upper (morphing) and low surfaces of the tunnel and the top of the cowl plate. In this realization the surface is morphed as shown in Fig. 6. The model predicts that the insertion of the inlet into the top of the wind tunnel test section will not choke the wind tunnel, although there is a significant subsonic region at the bottom of the tunnel below the inlet where the cowl shock interacts with the lower boundary layer.

The boundary layer at the top ramp of the inlet is thick due to the fact that it has grown along the wind tunnel wall throughout the expansion. This thick boundary layer and the elliptical intersection of the inlet ramp with the round surface of the tunnel

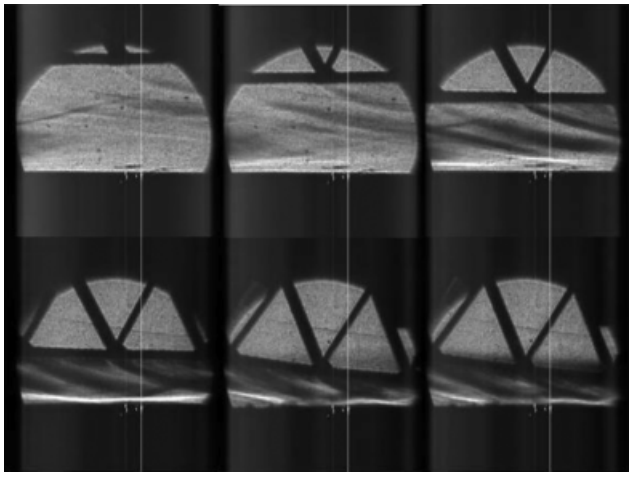

Fig. 8. Schlieren images of the flow during compression. Images are taken at 1.6-s intervals starting at 34.1 s into the run and show a 1.85 in. (4.7 cm) long section of the flow path. The weak shock structure from the upper (morphing) surface arises from the slight bumps in the woven ceramic associated with the connector pin locations.

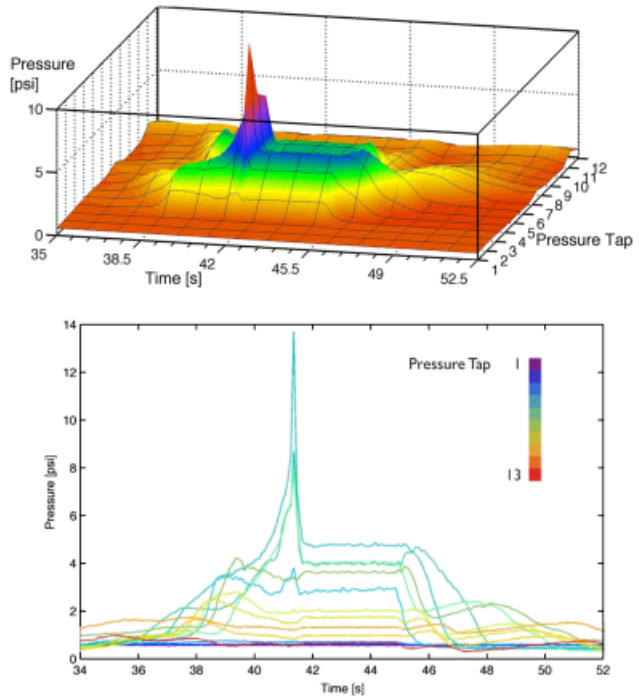

Fig. 9. Pressure versus time plots for the 13 pressure taps. Tap #1 is farthest upstream. The rapid pressure drop at 41.6 s corresponds to the slippage of an actuator due to the high surface pressure loading at maximum compression.

cause the shock from the 7° inlet ramp to be curved and unsteady, and thus not seen with schlieren imaging across the flow. The dashed ellipse in Fig. 7(b) highlights the slow pressure rise along the upper compression ramp associated with this three-dimensional (3D) interaction. Even though the shock is not apparent from the modeled schlieren images, it does lead to a reduction of the centerline Mach number and an increase in the static pressure along the morphing surface and along the upper surface of the cowl plate, as noted in Fig. 7(b). The high-pressure peak at the leading edge of the cowl plate results from the small stagnation point at that location.

A 2D method of characteristics model of the centerline shock structure and pressure contour inside the morphing inlet was developed as an on-site working tool for direct comparisons with experimental data. By implementing the rotational method of characteristics due to Ferri,[17] the expected pressure profile resulting from the morphing surface contour could be rapidly calculated. The simulations were performed using an inverse-marching scheme with 60 characteristics and 10^3 stream-wise steps. As input to the model the pressure and Mach number were specified at the inlet using experimental data and isentropic flow relationships.

V. Results

Results are shown in Figs. 8 and 9 from a series of tests in which the CMC wall was morphed as shown in Fig. 3 between positions corresponding to $h = 30$ and 5 mm, reducing the area ratio between the inlet and throat by a factor of 6. Figure 8 shows a sequence of schlieren images of the morphing inlet. These images were taken at 1.6-s interval starting at 34.1 s after the start of the run. Figures 9(a) and (b) are renderings of the time evolution of the pressure tap measurements during the shape morphing, with tap #1 the farthest upstream and tap #13 the farthest downstream. It is apparent that the morphing continued until the maximum pressure reached 13.7 psi (94.5 kPa), at which point the force on the actuators exceeded their load capacity and slippage occurred, immediately reducing the compression. The force on the central actuator at this point was estimated by multiplying the maximum pressure with the area supported by the central actuator (approximately 10 cm × 5 cm, or 4 in. × 2 in.), which results in a load of over 100 lbf (445 N). Subsequent static load tests indicated the actuators slip with a force of approximately 108 lbf (480 N).

The static pressure of 0.5 psi (3.4 kPa) in the unmorphed condition indicates that the Mach number of the flow through the inlet is 6.3. This is below the Mach 8 free stream condition due to the shock and compression waves from the front of the compression ramp and the leading edge of the cowl. Other weak shock structure in the facility upstream of the test section may also contribute to the reduction of the inlet Mach number. At the maximum displacement, the area ratio is approximately a factor of 6. The thickness of the boundary layer along the morphing surface can be estimated from the curvature of weak shocks visible in the in the schlieren images. These shocks were generated from small distortions of the woven ceramic plate beneath the actuator attachment points. The slope of these weak shocks can be used to approximate the local Mach number. These weak shocks show the Mach number increasing away from the wall and approaching the free stream angle. In the unmorphed condition, they reach the free stream angle at about 10 mm from the morphing surface. This corresponds to about 30% of the cross sectional area. In the highly deflected cases, the boundary layer shrinks due to compression, but occupies a larger fraction of the flow cross section, leading to an increase in the effective compression area ratio between the undeflected and fully deflected configurations. There is only a thin laminar

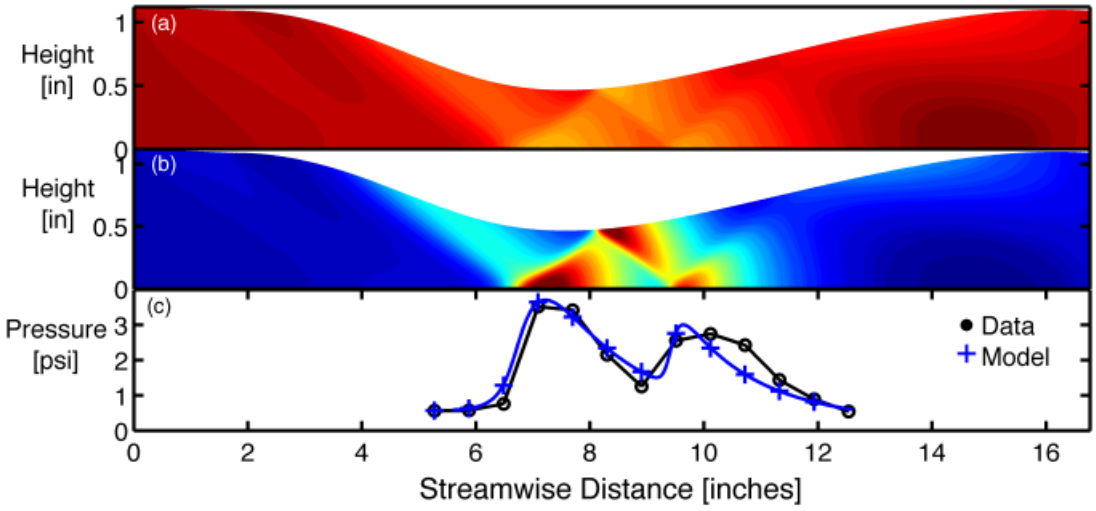

Fig. 10. Computed Mach number (a) and pressure (b) fields for inlet Mach number of 6.3 and computed and measured cowl wall pressure profiles (c).

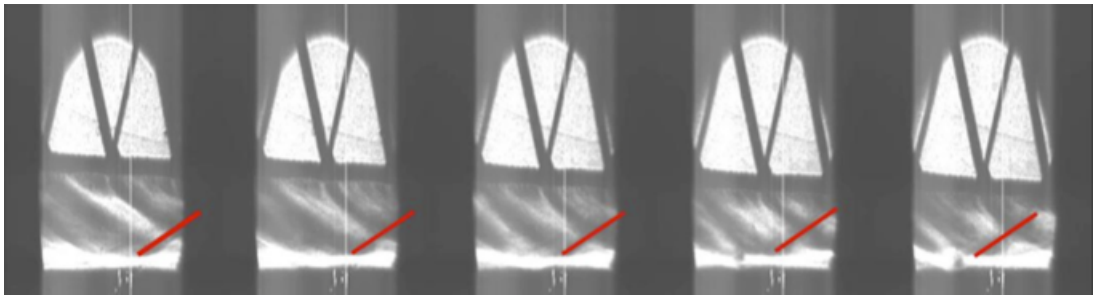

Fig. 11. Schlieren images taken at 0.2-s intervals showing the upstream advance of the reflected shock. The middle image corresponds to the 38.9 s point corresponding to the computed result in Fig. 10. The images show a 1.9 in. (4.7 cm) long length of the test section and are stretched to match the geometry of Fig. 10.

boundary layer on the cowl surface (lower plate) because the cowl lip is in the tunnel free stream and thus does not ingest the tunnel wall boundary layer.

The results of the analysis by the 2D method of characteristics for one snapshot during the experiment at $t = 38.9$ s are shown in Fig. 10. This time step was chosen about 2 s before the maximum compression point to avoid the region with multiple reflected shocks and associated increased unsteadiness. Figures 10(a)–(c) show calculated contours of Mach number and static pressure (a and b) as well as the computed pressure profile along the bottom surface (c). Also shown in Fig. 10(c) is the measured pressure profile from Fig. 9 at the 38.9 s point. The best fit to the data corresponds to an entrance Mach number of 6.3, as expected from the unmorphed pressure measurements. Five schlieren images taken at 0.2 s intervals over from 39.4 to 40.2 s are shown in Fig. 11, with the images distorted to match Fig. 10 and the contrast enhanced. The weak reflected shock is indicated with a red line in each frame and can be seen advancing upstream as the compression increases. The middle image is closest to the 39.8 s point corresponding to the computed result.

Figure 12 shows nine sequential schlieren images taken during the steady operation plateau from 42 to 44 s in Fig. 9. Note here that the morphing structure stays firmly in place with no observable shape fluctuations in the plate even between the pin joints. The weak shocks generated at the pin locations are evident and their local slopes provide a measure of local Mach number, which is about Mach 2.4 in the center of the flow for this configuration.

These results show that, other than the actuator slippage that occurred at the highest compression, the shape-morphing material provided reliable inlet shape control and had sufficient strength and stiffness to maintain the designated profile even in the presence of significant temperature gradients and pressure variations. Even with the small irregularities in the surface the overall performance of the morphing surface is in good agreement with predicted values.

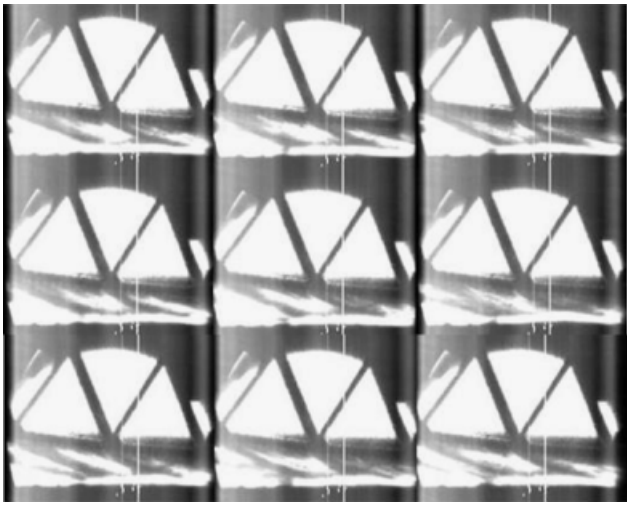

Fig. 12. Sequential 0.2 s images of constant geometry morphed surface showing steady plate contour. The visible section is 1.9 in. (4.7 cm) long in the horizontal direction.

VI. Conclusions

The development of CMCs with integrally woven fiber reinforcements has led to the potential for active shape morphing of surfaces in high temperature and variable pressure environments. Large temperature and pressure gradients can be sustained without significant distortion of the shape. For the experiments reported here a 0.7 mm thick, 37.5 cm long, and 11 cm wide plate of C–SiC composite was connected to an actuated truss structure and mounted as the upper surface of a shape-morphing hypersonic inlet. The lower surface was a flat steel plate instrumented with an array of pressure taps. The operation of this morphing inlet in an 800 K, 9 in. (23 cm) diameter Mach 8 wind tunnel facility demonstrated that the actuator-controlled CMC surface could be shaped to a desired contour and maintained at that contour in the presence of significant temperature gradients and pressure loads. The measured pressure profile matched the computed profile to good accuracy. The integrally woven pin-joint attachment method proved robust, although there were weak shock waves observed emanating from the slight distortions of the front surface at the attachment locations. These distortions can be easily eliminated in future developments. The actuators accurately controlled the surface contour until the back-pressure force rose above 100 lbf (445 N) per actuator, the limit of the actuator operation envelope, and at that point some slippage occurred. These results demonstrate that textile-based CMCs are excellent candidates for applications in hypersonic vehicles and hypersonic ground test facilities, where large variations in shape and accurate shape control are required in the presence of severe temperature and pressure loads.

References

[1]E. T. Curran, and S. N. B. Murthy (eds.), *Scramjet Propulsion, Progress in Astronautics and Aeronautics*, Vol. 189. Paul Zarchan, Editor in Chief AIAA, Reston, VA, 2000.

[2]C. R. McClinton, "High Speed/Hypersonic Aircraft Propulsion Technology Development"; pp. 1-1 to 1-32 in *Advances on Propulsion Technology for High-Speed Aircraft. Educational Notes RTO-EN-AVT-150, Paper 1*. RTO, Neuilly-sur-Seine, France, 2008. Available at http://www.rto.nato.int

[3]P. Balakumar, H. Zhao, and H. Atkins, "Stability of Hypersonic Boundary-Layers over a Compression Corner"; AIAA Paper No. 2002-2848, June 24–26, 2002.

[4]R. J. Engers, D. R. Rubin, F. Marconi, and A. F. Bartlett, "Missile Radome Development Testing at ATK GASL"; AIAA 2007-1649, 2007.

[5]K. H. Timpano, S. Zaidi, L. Martinelli, and R. B. Miles, "Design and Test of a Morphing Supersonic Nozzle"; AIAA Paper No. 2008-851, 48th AIAA Aerospace Sciences Meeting and Exhibit. Reno, NV, 2008.

[6]M. Hagenmaier, D. Eklund, and R. Milligan, "Improved Simulation of Inlet Distortion Effects in a Direct-Connect Scramjet Combustor"; AIAA-2011-233.

[7]S. L. dos Santos e Lucato, J. Wang, P. Maxwell, R. M. McMeeking, and A. G. Evans, "Design and Demonstration of a High Authority Shape Morphing Structure," *Int. J. Solids Struct.*, **41** [13] 3521–43 (2004).

[8]S. L. dos Santos e Lucato and A. G. Evans, "The Load Capacity of a Kagome Based High Authority Shape Morphing Structure," *Trans. ASME*, **73**, 128–33 (2006).
[9]J. Wang, A. Nausieda, S. L. dos Santos e Lucato, and A. G. Evans, "Twisting of a High Authority Morphing Structure," *Int. J. Solids Struct.*, **44** [9] 3076–99 (2007).
[10]R. G. Hutchinson, N. Wicks, A. G. Evans, N. A. Fleck, and J. W. Hutchinson, "Kagome Plate Structures for Actuation," *Int. J. Solids Struct.*, **40**, 6969–80 (2003).
[11]T. J. Lu, J. W. Hutchinson, and A. G. Evans, "Optimal Design of a Flexural Actuator," *J. Mech. Phys. Solids*, **49**, 2071–93 (2001).
[12]V. S. Deshpande and N. A. Fleck, "Collapse of Truss Core Sandwich Beams in 3-Point Bending," *Int. J. Solids Struct.*, **38**, 6275–305 (2001).
[13]D. B. Marshall and B. N. Cox, "Integral Textile Ceramic Structures," *Annu. Rev. Mater. Res.*, **38**, 425–43 (2008).
[14]S. Flores, A. G. Evans, F. W. Zok, M. Genet, B. N. Cox, D. B. Marshall, O. Sudre, and Q. Yang, "Treating Matrix Nonlinearity in the Binary Model Formulation for 3D Ceramic Composite Structures," *Compos.: Part A*, **41**, 222–9 (2010).
[15]S. F. Shuler, J. W. Holmes, X. Wu, and D. Roach, "Influence of Loading Frequency on the Room Temperature Fatigue of a Carbon-Fiber/SiC-Matrix Composite," *J. Am. Ceram. Soc.*, **76** [9] 2327–36 (1993).
[16]J. W. Holmes, "Influence of Stress Ratio on the Elevated-Temperature Fatigue of a Silicon Carbide Fiber-Reinforced Silicon Nitride Composite," *J. Am. Ceram. Soc.*, **74** [7] 1639–45 (1991).
[17]A. Ferri, "The Method of Characteristics for the Determination of Supersonic Flow Over Bodies of Revolution at Small Angles of Attack"; NACA Report No. 1044, 1951. □